J Mater Sci (2010) 45:523–532
DOI 10.1007/s10853-009-3970-1

Dislocation motion in the early stages of high-temperature low-stress creep in a single-crystal superalloy with a small lattice misfit

J. X. Zhang · H. Harada · Y. Koizumi · T. Kobayashi

Received: 4 August 2009 / Accepted: 8 October 2009 / Published online: 7 November 2009

Abstract Dislocation configurations at different creep stages (1100 °C and 137 MPa) in a superalloy TMS-75(+Ru) were studied in transmission electron microscopy (TEM) and the movement path of these creep-produced dislocations could be fully illustrated. Due to the small value of γ/γ' lattice misfit, these dislocations cannot glide in the horizontal γ matrix channels by cross slip, but they mainly move by climbing around the γ' cuboids. In the primary stage, the dislocations first move by slip in the γ-matrix channels. When they reach the γ' cuboids, they move by climbing along the γ' cuboid surfaces. In the secondary creep stage, dislocation reorientation in the (001) interfacial planes happens slowly, away from the deposition orientation of $\langle 110 \rangle$ to the misfit orientation of $\langle 100 \rangle$. The velocity of the reorientation is lower and a perfect γ/γ' interfacial dislocation network cannot be formed quickly. This factor results in a large creep rate of the alloy during the secondary creep stage. The path for dislocation motion during the early creep stages consists of the following sequences: (i) climbing along the γ' cuboid surface, (ii) deposition onto the (001) γ/γ' interfacial plane, and (iii) reorientation from the $\langle 110 \rangle$ direction to the $\langle 100 \rangle$ direction.

J. X. Zhang (✉)
Key Laboratory of Liquid Structure and Heredity of Materials (Ministry of Education), School of Materials Science and Engineering, Shandong University, 73 Jingshi Road, Jinan, Shandong Province 250061, China
e-mail: jianxin@sdu.edu.cn

J. X. Zhang · H. Harada · Y. Koizumi · T. Kobayashi
National Institute for Materials Science, 1-2-1 Sengen, Tsukuba, Ibaraki 305-0047, Japan

Introduction

Nickel-based superalloys are important materials used in advanced high-temperature components such as turbine blades in gas engines [1, 2]. The high-temperature strengths of these nickel-based alloys result from hardening by a high-volume fraction of ordered coherent γ' particles [3]. These particles can arrest or slow down the mobile dislocations and extensive deformation cannot occur unless a minimum stress is applied so that the dislocations can escape from the pinning particles [4]. The dislocations overcome the particles by: (a) particle shearing, (b) Orowan bowing, (c) climb around particles, and (d) drag of particles. The particle shearing tends to happen at low-temperature with high-stress, Orowan bowing can be found in alloys with a low-volume fraction of particles, and climbing motion can be found in high-temperature low-stress creep [3–8].

With the development of superalloys, single crystal superalloys strengthened by a high-volume fraction of ordered cuboidal γ' particles in the face-centered cubic γ matrix became dominant in this field [9, 10]. Since the creep resistance of these γ/γ' alloys is much higher than that of either the γ or γ' materials in the bulk form, it is clear that the two-phase microstructure is very important in building up the high-level of strength. Creep of such single-crystal superalloys have been extensively studied over the past decade [9, 10]. The majority of microstructural studies concentrate on the low-temperature high-stress creep deformation [9–17].

So far, there are also a lot of work on the dislocation mechanisms which govern high-temperature low-stress creep [18–26]. Especially in alloys with small lattice mismatch, dislocation climb is a main deformation mode in the early stages of creep. Until now there is still some

experimental work on the details of the climbing dislocations in superalloys during the tensile creep deformation along the [001] direction. In fact, this process is considerably important for understanding the creep resistance.

This article is concerned with the dislocation movement during creep (1100 °C and 137 MPa) in a modern superalloy having a small lattice mismatch. In particular, dislocation climbing in the early stages of creep is described, based on experimental observations and stereographic analysis of dislocation configurations.

Experimental

Single crystal superalloy TMS-75(+Ru) was used in the form of cast rods having an axial orientation within 10° of [001] direction. The alloy TMS-75(+Ru) is an alloy designed based on a third generation single-crystal superalloy TMS-75 with the addition of Ru [27]. The chemical composition of the TMS-75(+Ru) alloy is listed in Table 1. After a two-step solution heat treatment of 1300 °C for 1 h, plus 1320 °C for 5 h, a two-step aging treatment of 1150 °C for 4 h, plus 870 °C for 20 h was followed. This heat treatment produces a microstructure containing about 65% cuboidal γ' precipitates, which are on average 0.35 μm in size along the cube edge.

Creep-test specimens were machined from solidified single-crystal bars. These specimens had a gauge length of 22 mm and a diameter of 4 mm. Creep tests were carried out at 1100 °C and 137 MPa. One specimen was tested until rupture. The other specimens were interrupted after 2, 4, 20, and 60 h of creep test, respectively, and were cooled under load to preserve the dislocation arrangements. Specimens for TEM observation were cut perpendicularly to [001]. To get a stereographic view of the dislocation configuration in the specimen interrupted at 20 h, this specimen was cut along the (112) plane (i.e., intersection with the rafted γ/γ' structure). After mechanically grinding, TEM foils were electrochemically thinned in a solution of 80 mL perchloric acid, 20 mL ethanol, and 400 mL 2-Butex ethanol at 3 °C. Stereomicroscopy techniques were used extensively to obtain the arrangement details of dislocations.

Table 1 Chemical composition of TMS-75(+Ru) (wt%)

Co	Cr	Mo	W	Al	Ta	Hf	Re	Ru	Ni
12	3	2	6	6	6	0.1	5	1.6	Bal.

Results

Creep curve

A typical creep curve of the superalloy TMS-75(+Ru) tested at 1100 °C under 137 MPa is shown in Fig. 1a. After 20 h, the creep is in a secondary stage. The creep rupture life is about 142 h. According to the comparison made with other superalloys [27], this alloy has a relatively high creep rate in the secondary creep stage and wide γ/γ' interfacial dislocation spacing. The X-ray measurement showed the γ/γ' lattice misfit in the alloy was about −0.16% (measured at 1100 °C, before creep test). This misfit value is very small relative to the reported γ/γ' lattice misfit (approx. −0.3%) in the modern nickel-base single crystal superalloys [9, 10, 27, 28]. According to the previous evaluation [28], the stress field in this alloy cannot push the dislocations to move into the horizontal γ matrix channels by cross slip. Thus, during creep a possible movement by climbing around the γ' cuboids is expectable.

The creep curve for the initial 20 h is also given in Fig. 1a, as shown by the inset. The creep strain increases slightly during the first 2–3 h. After 5 h of creep, the strain increases rapidly.

Figure 1b shows the relationship between the strain and the creep rate. When the strain is small, the creep rate is also very small. It is difficult to find the accurate dependence of creep rate on the strain from this figure in the scope of small strain. Generally speaking, the creep rate is very small in the primary creep stage and in the secondary

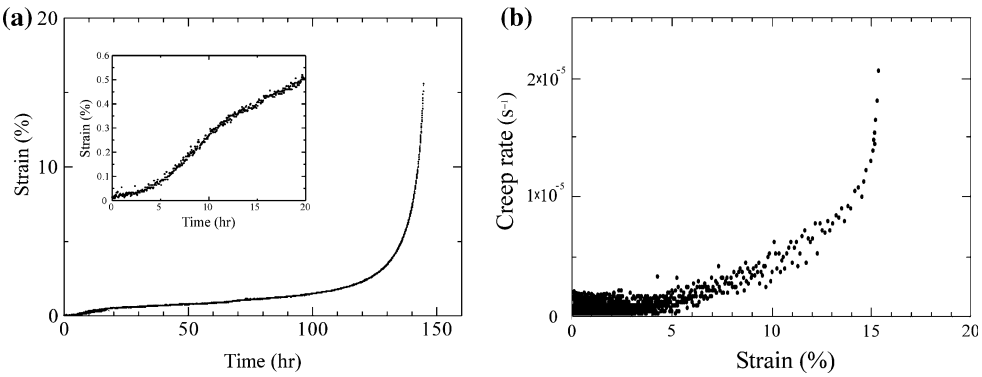

Fig. 1 **a** Creep curve of TMS-75(+Ru) tested at 1100 °C and 137 MPa. A segment of the creep curve for the initial 20 h is shown in the inserted. **b** Creep rate–strain relationship of the superalloy tested at 1100 °C and 137 MPa

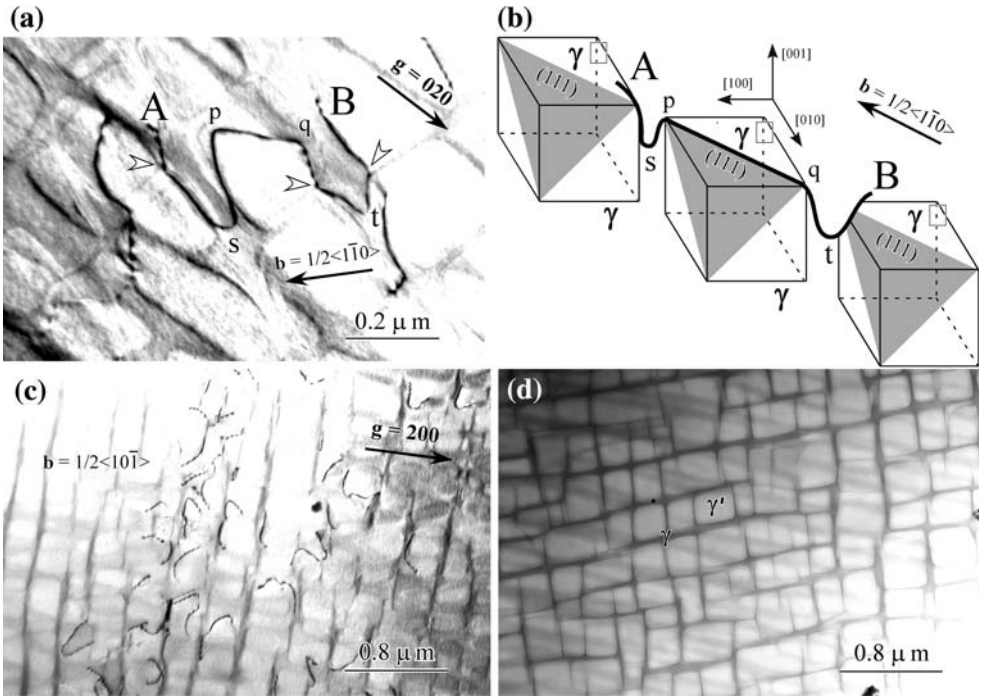

Fig. 2 Configuration of dislocations in the specimen interrupted after 2 h of creep. **a** A screw dislocation AB is gliding in a (111) plane in γ channels, with its segment pq meeting the upper surface of a γ' cuboid and its other two parts bowing into γ channels at sites 's' and 't'. Beam//[001]. **b** A schematic illustration to show the stereoscopic configuration of the dislocation AB in (**a**). **c** General morphology of dislocations in γ channels. Beam//[011]. **d** Most of the area is free of dislocations. Beam//[001]

creep stage. The creep rate increases drastically in the tertiary creep stage.

Configuration of dislocations after 2 h of creep test

Figure 2a and c show the microstructure of a specimen interrupted after 2 h of creep. In Fig. 2a, a dislocation AB is gliding into γ channels as manifested by its bowed dislocation segments shown at "s" and "t". One part (pq) of the dislocation was stopped at the surface of a γ' cuboid. In addition, there are "bulges" along the dislocation line as marked by the arrows. These bulges have also been found to exist in the specimen (CMSX-3) during an incubation period when tested at 825 °C and 450 MPa [9]. This is one mode of lateral dislocation spreading into the intersecting γ-matrix channels. When the dislocation moves in the channels in one orientation, it may try to spread into the channels in another orientation at positions indicated by the arrows. In Fig. 2b, the movement of the dislocation into the γ/γ' structure is shown schematically. The screw dislocation having Burgers vector $\mathbf{b} = a/2[1\bar{1}0]$ was moving in the (111) plane. A section of the dislocation line was stopped at pq and the rest was trying to spread into the γ channels.

The observation of an $a/2[1\bar{1}0]$ dislocation is rare because of its unfavorable Schmid factor. Its appearance may be caused by the misalignment of the tensile axis from [001]. The dislocations having Burgers vectors $\mathbf{b} = a/2[10\bar{1}]$ and $\mathbf{b} = a/2[101]$ are shown in Fig. 2c. From their morphology, these dislocations are different from the $a/2[1\bar{1}0]$ dislocation in Fig. 2a. In general, an $a/2[1\bar{1}0]$ screw dislocation tends to have a considerable length in the TEM sample [thin film parallel to the (001) plane]. However, for the $a/2\langle 10\bar{1}\rangle$ dislocations in Fig. 2c, segments were observed because these dislocations were oriented at an angle to the foil surface.

When the creep test was carried out for 2 h, the distribution of dislocations in the observed specimen was not homogeneous. Most of the area was free of dislocations as shown in Fig. 2d. That is to say, a limited number of dislocation sources were being operated. This observation is consistent with the slow increase in creep strain (Fig. 1) over the initial 2–3 h.

Configuration of dislocations after 4 h of creep test

Figure 3a through f show the morphologies of dislocations in a specimen interrupted after 4 h of creep test. Six groups of dislocations (with different amounts in each group) are characteristically marked and further magnified. The dislocation segments in group '1' are typically inclined relative to the plane (001) as manifested by their dotted appearance and gradual increase in length by tilting the specimen toward [011]. The dislocations in group '2' are bowing along the edge of a γ' cuboid. They almost become straight lines when viewed in the [011] direction, as shown in Fig. 3d and f. The dislocations in groups '3' and '4' show other interactions between gliding dislocations and γ' cuboids. These dislocations are approaching the γ' cuboids. The dislocation in group '5' is moving to the cuboid and

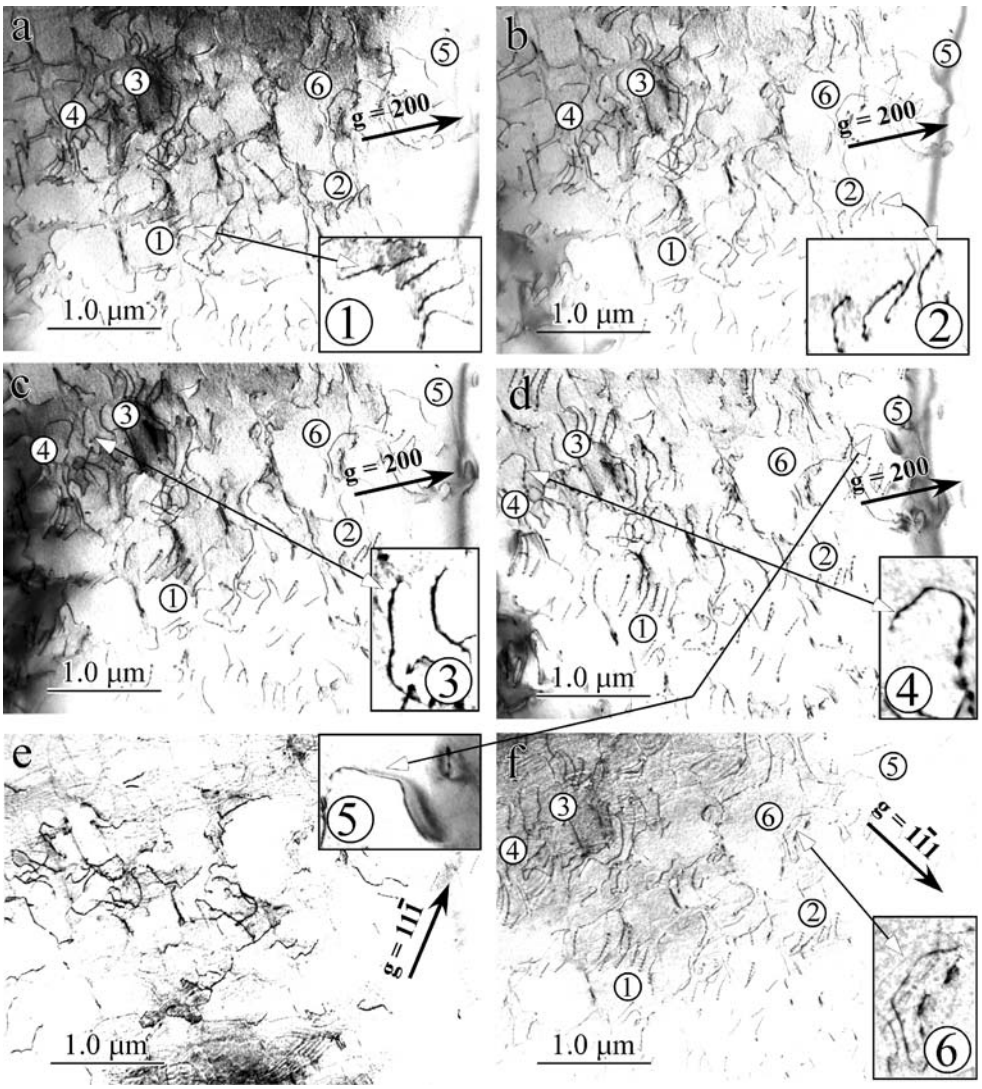

Fig. 3 Two-beam bright-field images showing morphologies of dislocations during tilting specimen in TEM (The specimen was interrupted after 4 h of creep). **a** Beam//[001]. **b** Beam//[013]. **c** Beam//[012]. **d**, **e**, **f** Beam//[011]. Several dislocation configurations are marked by figures and the framed parts are their further magnification. See the text for details

intersects it at a special position as analyzed below. The dislocation in group '6' is an $a/2[1\bar{1}0]$ dislocation, which is spreading around a γ' cuboid.

Figure 4 is a schematic illustration to show the intersection of a {111} slip plane with a γ' cuboid. For a *fcc* structure, there are eight equivalent {111} slip planes (in Fig. 4a, four {111} planes are drawn in the upper half of a cube). In Fig. 4b–d, particular attention is given to, and the illustrations show, the possible intersection cases of octahedral slip dislocations with a γ' cuboid in the (111) plane when the tensile axis is along the [001] direction. In Fig. 4b, a dislocation a_1b_1 approaches the cuboid at a broad side plane (100), and its impinging segment is shown in the sketch. After deposition, the dislocation a_1b_1 may climb or glide in the (100) plane to the top point T of the (111)-plane-based tetrahedron. On the other hand, if a dislocation c_1d_1 approaches the cuboid at its edge as shown in Fig. 4b, it will climb to the top point T of the tetrahedron along the edge. In Fig. 4c, the movement of the dislocations a_2b_2 and c_2d_2 is in a similar way to that of the dislocations a_1b_1 and c_1d_1 (Fig. 4c), respectively.

In Fig. 4d, all the possible cases of the intersection of the (111) plane with a γ' cuboid are drawn for the dislocations having a significant resolved stress when loaded along the [001] axis. Above the plane ABC, the intersection plane is a triangle as marked in dark. Below the plane DEF, the intersection is also a triangle (in white, Fig. 4d). For these two cases, the encountering dislocations may climb to the top point T of the ABC-plane-based tetrahedron or the top point P of the DEF-plane-based tetrahedron. The intersections for positions between the planes ABC and DEF is slightly complex. In general, the intersection area is an irregular

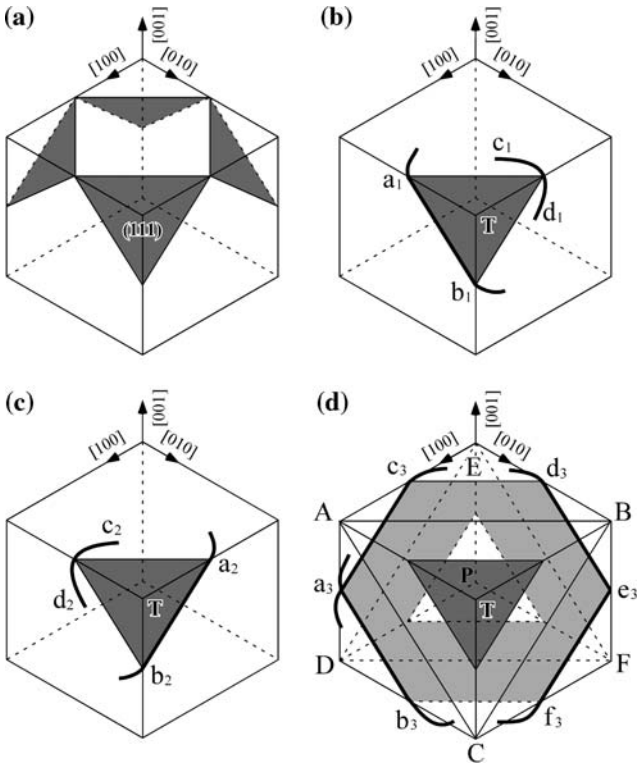

Fig. 4 Intersection geometry for dislocations on the octahedral glide planes with a γ' cuboid. **a** Four {111} glide planes in a γ' cuboid. **b**, **c** Configuration of dislocations intersecting with the γ' cuboid in a (111) plane. **d** Three cases of the intersection for the (111) plane with the γ' cuboid: the top is an *inverted triangle* (*dark*), the bottom is also a *triangle* (*blank*), and the intermediate part is a hexagon

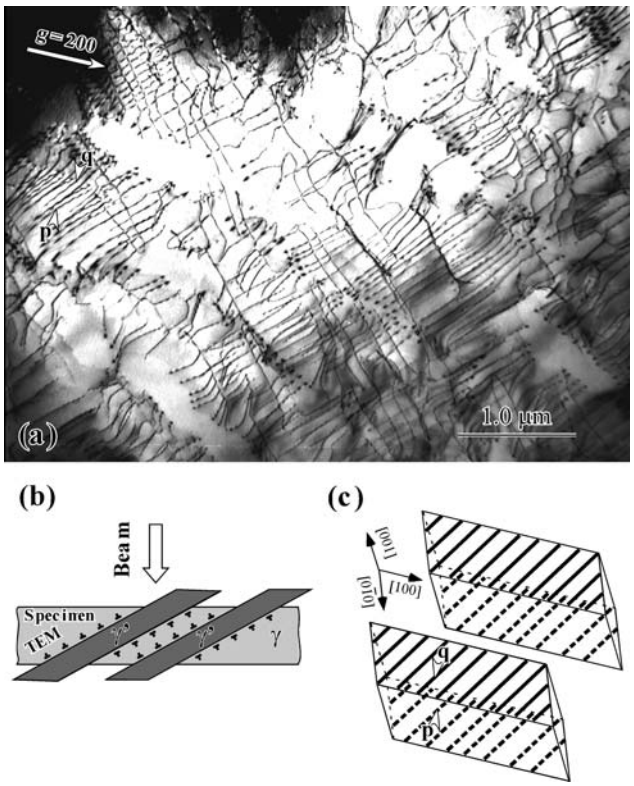

Fig. 5 **a** Morphology of dislocations in the specimen interrupted after 20 h of creep. Beam//[011]. **b** Schematic illustration of the TEM foil. **c** Schematic illustration of the overlapping γ/γ' interfacial dislocations in the upper and lower interfaces observed in (**a**)

hexagon having varying shapes at different heights, as shown by the light gray area in Fig. 4d. For the dislocation a_3b_3, it may climb to the point T in the (100) plane; the dislocation a_3c_3 may climb to the point P in the (010) plane. If the channels are wide enough, it is possible that an encountering dislocation may deposit more extensively onto the cuboid, as shown by the dislocation $d_3e_3f_3$ in Fig. 4d.

Based on stereographic analysis by tilting the specimen in the TEM, and by relating the intersection geometry of slip plane with a γ' cuboid, the dislocation configurations can be further understood. The dislocations in the groups (1), (3), and (4) in Fig. 3 are encountering their corresponding γ' cuboids along the {100} plane like the dislocations a_1b_1, a_2b_2, a_3b_3, and a_3c_3 in Fig. 4. The dislocations in the group (2) are reaching a cuboid along the edge of the cuboid like the dislocations c_1d_1 or c_2d_2 in Fig. 4. The morphology of the dislocation in the group (5) is not common and it is a case of the dislocation type $d_3e_3f_3$ in Fig. 4d. It must be pointed out that the dislocation line directions in Fig. 3 have deviated from their original $\langle 110 \rangle$ orientations into different angles due to their climb during creep at such a high-temperature (1100 °C). That is to say, most of the dislocations are in a non-screw configuration.

Configuration of dislocations after 20 h of creep test

The dislocation configurations after creep test for 20 h are shown in Fig. 5a. The dislocations are mainly oriented along the [110] and $[1\bar{1}0]$ directions. The overlapping of dislocations in the upper and lower surfaces of a γ' cuboid can be clearly seen in some regions. Since the specimen was not cut parallel to the (001) plane, the γ/γ' interfacial plane is inclined relative to the TEM foil plane as shown in Fig. 5b. So it is reasonable to find the overlapping dislocation arrays in projection for some regions as shown in Fig. 5c. For this to be understood more easily, two dislocation lines marked by the letters 'p' and 'q' in Fig. 5a are also marked by the same letters in the schematic drawing of Fig. 5c.

In Fig. 5a, the dislocations in two mutually perpendicular [110] and $[1\bar{1}0]$ directions, are not distributed with the same density. This is caused by the small misalignment of the specimen tensile axis from the [001] direction. This misalignment will lead to different Schmid factors for the {111} planes. That is to say, some slip systems can be more easily operated.

Figure 6 is a schematic illustration of the climb sequence and the subsequent deposition of the dislocations

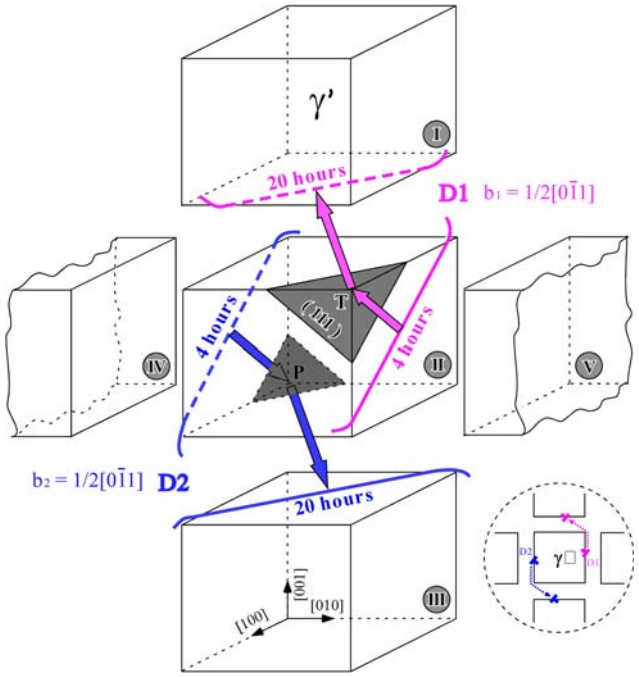

Fig. 6 Schematic illustration of dislocations' climbing along the (010) γ/γ' interfacial plane and then arriving at the (001) γ/γ' interfacial plane. The red and blue arrows show the movement trace of these two dislocations in the initial creep stage from 4 to 20 h. The circled area at the bottom right corner simply shows the movement trace of these two dislocations viewed from the [100] direction

at a horizontal γ/γ' interfacial plane. This figure shows the dislocation climb process approximately initiating from after 4 h of creep test to 20 h. Suppose dislocations D1 and D2 have the same Burgers vector $\mathbf{b} = 1/2[0\bar{1}1]$ and line direction u = $[10\bar{1}]$. As shown in the circled area, the dislocations D1 and D2 can relieve the negative misfit at the γ/γ' interface. If the dislocations D1 and D2 in the (111) plane are approaching the γ' cuboid 'II' from the right and the left, respectively, the dislocation D1 may climb to the point T and the dislocation D2 may climb to the point P. The dislocation D1 cannot stay on the upper surface of the γ' cuboid 'II', because it will adds to negative misfit there. Therefore, after getting over the top point T, the dislocation D1 will adjust its orientation to $[0\bar{1}1]$ due to the fact that a dislocation in a screw configuration has a low self-energy. The dislocation will glide in the (111) plane until it touches the (001) γ/γ' interfacial planes at the bottom of the γ' cuboid 'I' and deposits along a $[1\bar{1}0]$ direction. Similarly, the dislocation D2 may deposit onto the upper surface of the γ' cuboid 'III'.

Configuration of dislocations after 60 h of creep test

Figure 7a–f show the configuration of dislocations in a specimen extracted after 60 h of creep loading. At a glance, the dislocations orient themselves in the directions ranging from ⟨110⟩ to ⟨100⟩. In fact, most of the dislocation segments are in an inclined state in the TEM foil. Compared with the orientation of dislocations in the specimen interrupted after 20 h of creep test (Fig. 5), these dislocations are in the process of reorientation from the deposited dislocation line directions ⟨110⟩ to the ⟨100⟩ directions [29]. The reorientation proceeds differently for dislocations in different areas. This is related to two possible factors. One factor is that the misorientation of the specimen load axis leads to different Schmid factors for different slip systems and thus some systems can be easily operated during creep. The other is the generation of the γ/γ' rafted structure during creep, which makes the initially smooth γ/γ' interfacial planes become irregular, as shown in Fig. 8. In Fig. 8a, the γ/γ' rafted structure after 60 h of creep test was considerably broken up in comparison to the initially rafted structure after only 20 h (see the inset in Fig. 8a). Some γ/γ' interfacial habit planes develop that are severely inclined relative to the original (001) habit planes, as shown in the area marked by arrows in Fig. 8b. If one observes the interfacial dislocations in these inclined habit planes, the dislocations will have different orientations in different areas.

Now let us look back at the intersection of dislocations in the interfaces in Fig. 7. A group of dislocations (marked by 'A') in Fig. 7a is intersecting with another group of dislocations (marked by 'D') in Fig. 7b. The dislocation lines become zigzagged as a result of the intersection. Similarly, the dislocations (marked by 'F') in Fig. 7e are intersecting the dislocation 'G' in Fig. 7f, which results in zigzagged dislocation lines. The case is also similar with the dislocations 'B' and 'C' in Fig. 7a when they intersect the dislocations 'E' in Fig. 7b.

Figure 9a–d schematically shows the intersection of dislocations in the γ/γ' interfacial plane. At the intersection nodes, dislocation reactions take place. The original one node splits into two nodes connected by the product (bold bars in Fig. 9b, d). The dislocation reactions shown in Fig. 7 can be expressed as follows:

$$\mathrm{A} + \mathrm{D};\ \frac{1}{2}[101] + \frac{1}{2}[01\bar{1}] \rightarrow \frac{1}{2}[110] \quad (1)$$

$$\mathrm{F} + \mathrm{G};\ \frac{1}{2}[110] + \frac{1}{2}[\bar{1}0\bar{1}] \rightarrow \frac{1}{2}[01\bar{1}] \quad (2)$$

$$\mathrm{B} + \mathrm{E};\ \frac{1}{2}[101] + \frac{1}{2}[01\bar{1}] \rightarrow \frac{1}{2}[110] \quad (3)$$

$$\mathrm{C} + \mathrm{E};\ \frac{1}{2}[\bar{1}01] + \frac{1}{2}[01\bar{1}] \rightarrow \frac{1}{2}[\bar{1}10] \quad (4)$$

All the reactions above result in a reduction in $|b|^2$ from a^2 to $1/2a^2$ (where a is the lattice parameter), and thus these would be energetically favorable.

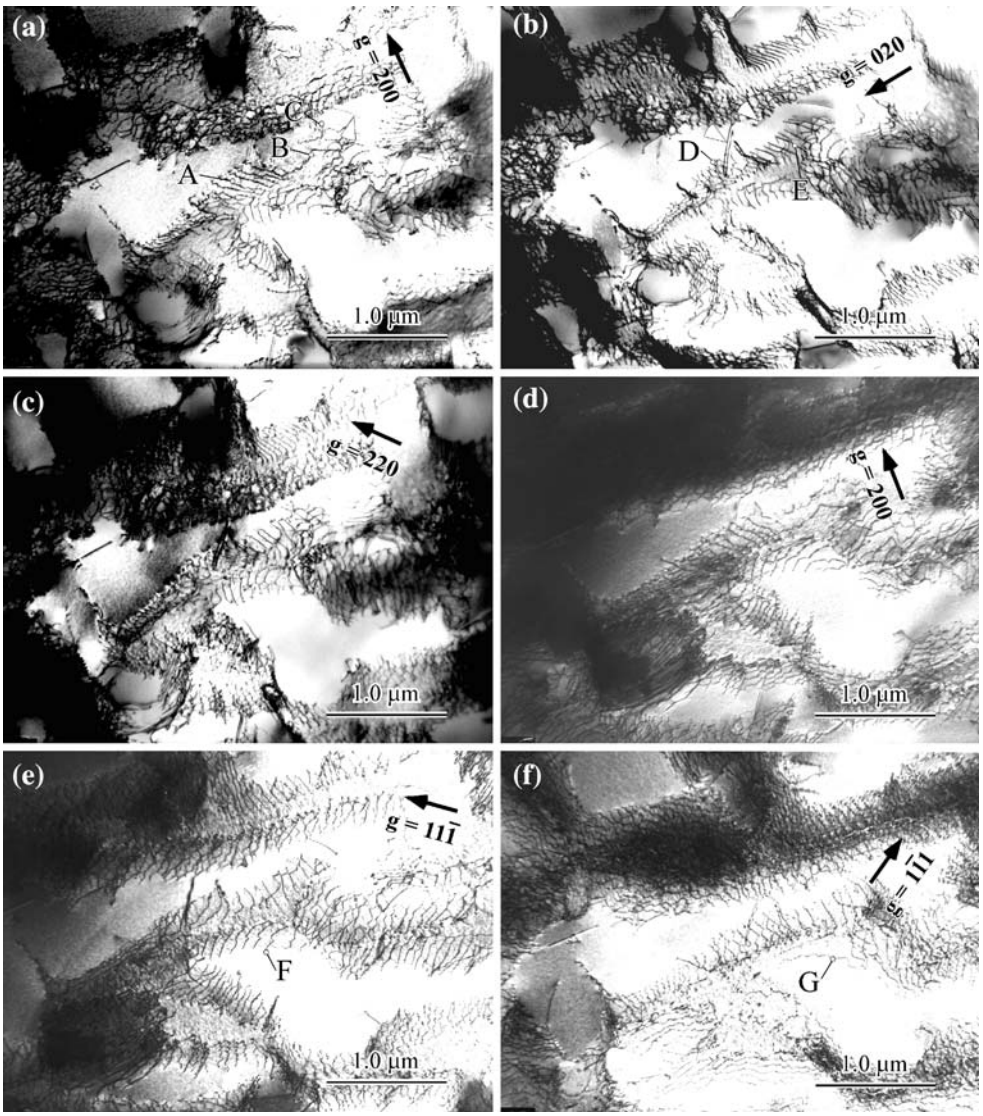

Fig. 7 Configurations of dislocations during tilting the specimen (from the test interrupted at 60 h). **a**, **b**, **c** Beam//[001], and (**d**, **e**, **f**) beam//[011]. Dislocation A: $\mathbf{b} = 1/2[101]$, B: $\mathbf{b} = 1/2[101]$, C: $\mathbf{b} = 1/2[\bar{1}01]$, D: $\mathbf{b} = 1/2[01\bar{1}]$, E: $\mathbf{b} = 1/2[01\bar{1}]$, F: $\mathbf{b} = 1/2[110]$, G: $\mathbf{b} = 1/2[\bar{1}0\bar{1}]$. Dislocation reactions take place between dislocations as characterized by zigzagged dislocation lines. One group of such zigzagged dislocation lines are shown by the inset in (**e**)

Configuration of dislocations after creep rupture

Figure 10 shows the morphology of dislocations after creep rupture. The dislocation lines align roughly along the mismatch directions [100] and [010]. At the nodes dislocation reactions take place and some new dislocations appear in the form of short segments that connect the old and the new meshes in the network. The details of the interfacial dislocation network after creep rupture have been described in our previous report [27]. If the dislocation line directions in Fig. 5 (20 h), Fig. 7 (60 h), and Fig. 10 (ruptured) are compared, it can be seen that a reorientation of dislocations from predominantly ⟨110⟩ directions to predominantly ⟨100⟩ directions in the γ/γ' interface accompanies the secondary creep stage.

Discussion

For modern nickel-base single-crystal superalloys, the lattice constant $a\gamma$ of the γ phase tends to be larger than that ($a_{\gamma'}$) of the γ' phase, and thus the γ/γ' lattice misfit is called a negative mismatch ($[a_{\gamma'} - a_{\gamma}]/2[a_{\gamma'} + a_{\gamma}] < 0$). During the tensile creep test, the applied stress is superimposed on the γ/γ' misfit stress, the net stresses are considerably different in the horizontal and vertical γ-phase channels [9]. The compressive stress is significantly higher in the horizontal channels than that in the vertical channels. Thus, the dislocations prefer to enter the horizontal γ channels. The motion mode of dislocations in the present alloy TMS-75(+Ru) is considerably different from that in the previous

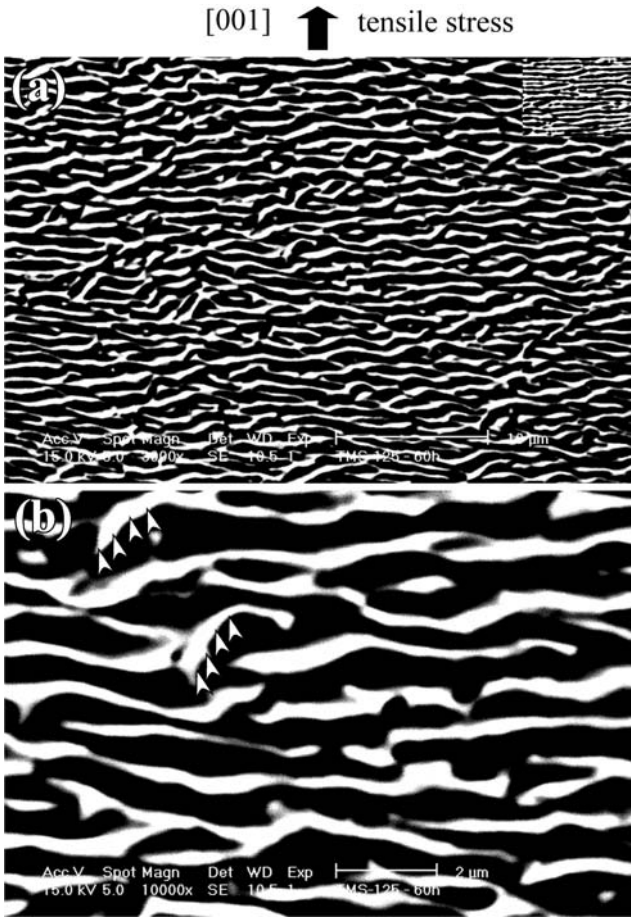

Fig. 8 The partially destroyed γ/γ' rafted structure at (**a**) a low magnification and (**b**) a high magnification in the specimen interrupted after 60 h of creep test. Some interfacial planes are strongly inclined relative to the initially rafted structure as marked by *arrows* in (**b**) (the inset in (**a**) shows a specimen interrupted after 20 h of creep test)

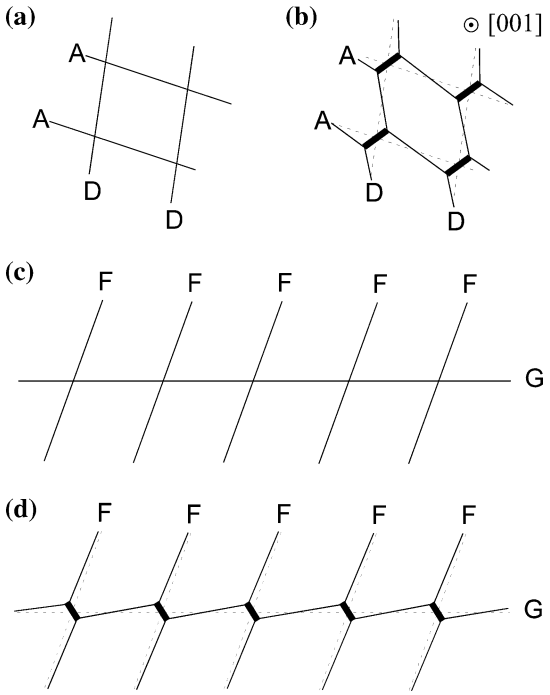

Fig. 9 Schematic illustration to show the deposition of glide dislocations (**a**, **c**) and subsequent reactions between these deposited dislocations (**b**, **d**). The *bold bars* at the intersections in (**b**) and (**d**) are the products of dislocation reactions. The *dashed lines* represent the dislocation lines before the reaction. (**a**, **b**) $A + D; 1/2[101] + 1/2[01\bar{1}] \rightarrow 1/2[110]$. (**c**, **d**) $F + G; 1/2[110] + 1/2[\bar{1}01] \rightarrow 1/2[01\bar{1}]$

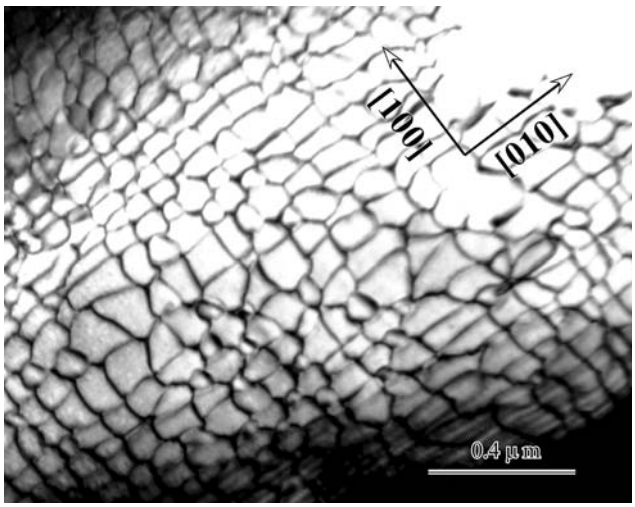

Fig. 10 Morphology of the γ/γ' interfacial dislocations after creep rupture. Beam//[001]

reports, such as CMSX-3 [9] and CMSX-4 [14]. In TMS-75(+Ru), the dislocations move mainly by climb along the γ/γ' interfaces during creep test. In contrast, the dislocations move mainly by cross slip in the horizontal γ-phase channels in CMSX-3 [9] and CMSX-4 [14]. One of the important factors is the difference in lattice misfit between the γ and γ' phases. For example, CMSX-3 at 850 °C has been estimated to have a misfit of −0.305% [9]. However, the misfits at 900 and 1100 °C measured by the X-ray method for the TMS-75(+Ru) alloy are −0.13 and −0.16%, respectively. The resolved shear stress for dislocation motion is supplied by the tensile stress and misfit stress, as shown in Fig. 11. If the resolved shear stress cannot overcome the Orowan resistance, the dislocations cannot enter the horizontal channels, as for dislocation 'A' in the figure. The dislocation will move mainly by climbing around the γ' cuboids as observed in the present study. In contrast, if a dislocation is able to overcome the Orowan resistance, it can penetrate through the horizontal γ-phase channels (as for dislocation 'B' in Fig. 11) and move by cross slip as observed for CMSX-3 [9] and CMSX-4 [14]. It should be pointed out that climbing or crossing slip of dislocations maybe exist simultaneously in a superalloy during high-temperature low-stress creep, and this

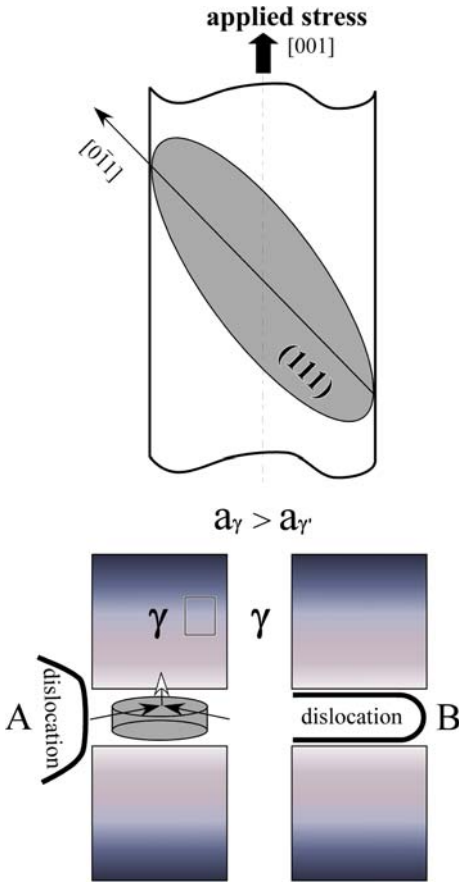

Fig. 11 Schematic illustration to show dislocation motion in the γ-phase channels. The upper part shows a $(111)[1\bar{1}0]$ slip system in the single-crystal specimen. The lower part shows the elastic stress due to a negative misfit between the γ and γ' phases

glide-climb process has been advocated by Carry and Strudel [30]. Certainly the leading movement mode of dislocations in a superalloy may vary in the light of the γ/γ' lattice misfit as discussed above.

Since the referenced test for CMSX-3 were carried out under low-temperature high-stress creep (850 °C, 552 MPa), it is clear that the high-tensile stress was likely a key factor for causing the dislocations to move into the horizontal γ-matrix channels. In fact, under the creep condition for TMS-75(+Ru) (1100 °C, 137 MPa), the dislocations may move by cross slip into the horizontal γ-matrix channels if the γ/γ' lattice misfit is large enough and negative. Recently, the creep process of another superalloy TMS-138 was studied under the same conditions as that of the TMS-75(+Ru) alloy. It was found that the dislocations in TMS-138 move typically by cross slip. An evaluation by the finite element method showed that the misfit stress caused by the large negative lattice mismatch, together with the external tensile stress, can overcome the Orowan resistance in TMS-138; but not in TMS-75(+Ru) (due to its small lattice misfit) [28].

Conclusions

The dislocation movement during creep testing at 1100 °C and 137 MPa in a superalloy TMS-75(+Ru) having a small γ/γ' lattice misfit, was described based on thorough transmission electron microscope observation for specimens taken from interrupted tests at different stages.

(1) In the primary stage, the dislocations first move by slip in the γ-matrix channels. When they reach the γ' cuboids, they move by climb along the γ' cuboid surfaces. Due to different intersection positions of the $\{111\}$ slip planes with the γ' cuboids, dislocations may finally deposit onto the bottom surface or top surface of the various γ' cuboids. With the operation of different slip systems, the interfacial dislocations are formed in the [110] and $[1\bar{1}0]$ directions on the (001) γ/γ' interfacial planes.

(2) In the secondary creep stage, dislocation reorientation in the (001) interfacial planes happens slowly, away from the deposition orientation of $\langle 110\rangle$ to the misfit orientation of $\langle 100\rangle$. The velocity of the reorientation is lower and a perfect γ/γ' interfacial dislocation network cannot be formed quickly. This factor results in a large creep rate of the alloy during the secondary creep stage. Meanwhile, dislocation reactions take place between these deposited dislocations, and form new dislocation segments. This contributes to the irregularity of the dislocation networks.

(3) In the superalloy TMS-75(+Ru), the dislocations move mainly by climb, rather than by cross slip commonly occurring in the horizontal γ-matrix channels in other superalloys. This is attributed to the small value of the γ/γ' lattice misfit in TMS-75(+Ru) alloy.

Acknowledgement This work was supported by the National Natural Science Foundation of China (Grant No. 50971078).

References

1. Reichman S, Duhl DN, Maurer G, Antolovich S, Laud C (1988) Superalloys 1988. The minerals. Metals & Materials Society, Warrendale, PA
2. Antolovich SD, Stusrud RW, MacKay RA, Anton DL, Khan T, Kissinger RD, Klarstrom DL (1992) Superalloys 1992. The minerals. Metals & Materials Society, Warrendale, PA
3. McLean M (1985) Acta Metall 33:545
4. Arzt E, Ashby MF (1982) Scr Metall 16:1285
5. Lagneborg R (1973) Scr Metall 7:605
6. Shewfelt RSW, Brown LM (1977) Phil Mag 35:945
7. Rosler J, Arzt E (1988) Acta Metall 36:1043
8. Kostka A, Malzer G, Eggeler G (2007) J Mater Sci 42:3951. doi: 10.1007/s10853-006-0166-9
9. Pollock TM, Argon AS (1992) Acta Metall Mater 40:1
10. Nabarro FRN, de Villiers HL (1995) The physics of creep. Taylor & Francis Publishers, London

11. Link T, Feller-Kniepmeier M (1992) Metall Trans A 23A:99
12. Sass V, Glatzel U, Feller-Kniepmeier M (1996) Acta Mater 44:1967
13. Feller-Kniepmeier M, Link T, Poschmann I, Scheunemann-Frerker G, Schulze C (1996) Acta Mater 44:2397
14. Sass V, Feller-Kniepmeier M (1998) Mater Sci Eng A A245:19
15. Matan N, Cox DC, Carter P, Rist MA, Rae CMF, Reed RC (1999) Acta Mater 47:1549
16. Ardakani MG, Mclean M, Shollock BA (1999) Acta Mater 47:2593
17. Rae CMF, Matan N, Cox DC, Rist MA, Reed RC (2000) Metall Mater Trans A 31A:2219
18. Mayr C, Eggeler G, Dlouhy A (1996) Mater Sci Eng A A207:51
19. Eggeler G, Dlouhy A (1997) Acta Mater 45:4251
20. Reed RC, Matan N, Cox DC, Rist MA, Rae CMF (1999) Acta Mater 47:3367
21. Srinivasan R, Eggeler GF, Mills MJ (2000) Acta Mater 48:4867
22. Shui L, Jin T, Tian S, Hu Z (2007) Mater Sci Eng A 454–455:461
23. Yeh AC, Rae CMF, Tin S (2004) In: Green KA, Pollock TM, Harada H, Howson TE, Reed RC, Schirra JJ, Walston S (eds) Superalloys 1992. The Minerals, Metals & Materials Society, Warrendale, PA, p 677
24. Svoboda J, Lukal P (1998) Acta Mater 46:3421
25. Mughrabi H (1996) In: Arsenault RJ, Cole D, Gross T, Sizek H, Liaw P, Parameswaran S, Kostorz G (eds) TMS Johannes Weertman symposium, 267 pp
26. Epishin A, Link T (2004) Phil Mag 84:1979
27. Zhang JX, Murakumo T, Koizumi Y, Kobayashi T, Harada H, Masaki S Jr (2002) Metall Mater Trans A 33A:3741
28. Zhang JX, Wang JC, Harada H, Koizumi Y (2005) Acta Mater 53:4623
29. Field RD, Pollock TM, Murphy WH (1992) In: Antolovich SD, Stusrud RW, MacKay RA, Anton DL, Khan T, Kissinger RD, Klarstrom DL (eds) Superalloys 1992. The Minerals, Metals & Materials Society, Warrendale, PA, p 557
30. Carry C, Strudel JL (1977) Acta Metall 25:767